Electronic Supplementary Material (ESI) for Materials Chemistry Frontiers.

Supporting Information

Polyoxometalate-Derived Bimetallic Catalysts for Nitrogen Reduction Reaction

Xiaohan Li[a,1], Cong Xue[a,1], Xinru Zhou[a,1], Yuao Wei[a], Yingjie Yu[a], Yu Fu[c], Wenjing Liu[,a], Yaqian Lan[*,b]*

[a] Key Laboratory of Flexible Electronics (KLOFE), Institute of Advanced Materials (IAM), Nanjing Tech University, 30 South Puzhu Road, Nanjing 211816, China

[b] School of Chemistry, South China Normal University, Guangzhou 510006, China

[c] Department of Chemistry, College of Sciences, Northeastern University, Shenyang 110819, China

[*]E-mails: iamwjliu@njtech.edu.cn, yqlan@m.scnu.edu.cn

Experimental Section

Reagents. Ultrapure water used throughout all experiments was purified through a Millipore system. All chemicals were analytically pure and used without further purification.

Synthesis of comparison samples:

1. Variation of calcination temperature to optimize Fe and Bi atomic ratio:

Synthesis of Bi/BiClO/Fe_3O_4-400, Bi/BiClO/Fe_3O_4-500, and Bi/Fe_3O_4-700

The synthesis of Bi/BiClO/Fe_3O_4-400, Bi/BiClO/Fe_3O_4-500, and Bi/Fe_3O_4-700 was similar to the above Bi/BiClO/Fe_3O_4-600, expect that the calcination temperature was changed to 400, 500, and 700 ^oC, respectively.

2. Synthesis of monometalic components to explore the source of activity:

Synthesis of Fe_3O_4

In a typical synthesis,[1] 15.2 g (56 mmol) $FeCl_3 \cdot 6H_2O$ and 7.7 g (27 mmol) $FeSO_4 \cdot 7H_2O$ were first dissolved in 300 mL of water, and then 25 ml of $NH_3 \cdot H_2O$ was added to the solution. The mixture was then stirred for 30 min at 90 °C. After the mixture was cooled to room temperature and filtered, the black precipitate of Fe_3O_4 was collected and washed 3 times with ultrapure water to remove excess ammonia and finally with acetone to remove excess water. The sample denoted as Fe_3O_4 was dried overnight in vacuum oven.

Synthesis of Bi/BiClO

The iron-oxo Keggin was calcinated in Ar with a temperature ramp from room temperature to

300 °C at a heating rate of 5 °C min^{-1}. The sample was held at 300 °C for 4 h, followed by naturally cooling to room temperature. After washing with ultrapure water, the sample denoted as Bi/BiClO was dried overnight in vacuum oven.

3. The precursors were changed from POMs to metal salts to verify the importance of introducing POMs:

Synthesis of Fe_2O_3 without adding Bi source

The synthesis of Fe-based precursor was similar to the above Bi_6Fe_{13}, expect that $Bi(NO_3)_3 \cdot 5H_2O$ was not introduced. After that, the Fe-based precursor was calcinated in Ar with a temperature ramp from room temperature to 600 °C at a heating rate of 5 °C min^{-1}. The sample was held at 600 °C for 4 h, followed by naturally cooling to room temperature. After washing with ultrapure water, the sample denoted as Fe_2O_3 was dried overnight in vacuum oven.

Synthesis of ternary bismuth composites without adding Fe source

The synthesis of Bi-based precursor was similar to the above Bi_6Fe_{13}, expect that $Fe(NO_3)_3 \cdot 9H_2O$ was not introduced. After that, the Bi-based precursor was calcinated in Ar with a temperature ramp from room temperature to 600 °C at a heating rate of 5 °C min^{-1}. The sample was held at 600 °C for 4 h, followed by naturally cooling to room temperature. After washing with ultrapure water, the sample denoted as $Bi/Bi_2O_3/Bi_{12}Cl_{17}O_{12}$ was dried overnight in vacuum oven.

Synthesis of iron-bismuth composites without adding $NaHCO_3$

The synthesis of Fe/Bi-based precursor was similar to the above Bi_6Fe_{13}, expect that $NaHCO_3$ was not introduced. After that, the Fe/Bi-based precursor was calcinated in Ar with a temperature

ramp from room temperature to 600 °C at a heating rate of 5 °C min^{-1}. The sample was held at 600 °C for 4 h, followed by naturally cooling to room temperature. After washing with ultrapure water, the sample denoted as $Fe_2O_3/Bi/Bi_2O_3/Bi_{12}Cl_{17}O_{12}$ was dried overnight in vacuum oven.

Characterizations

The powder X-ray diffraction (XRD) of samples were performed in Rigaku SmartLab, using Cu Kα radiation (λ = 1.5406 Å). The scanning electron microscopy (SEM) images were recorded by JSM-7800F of JEOL Ltd. The transmission electron microscopy (TEM) images were taken by JEM-2100F. The 2100F coupled with energy dispersive X-ray (EDX) spectroscopy was used. The Brunauer-Emmett-Teller (BET) specific surface area and porosity of the synthesized materials were analyzed using a physical adsorption analyzer model ASAP 2460 from Micromeritics. The X-ray photoelectron spectroscopy (XPS) was tested by Thermo Fisher Scientific D 250Xi. The absorbance data were measured with an ultraviolet-visible (UV-vis) spectrophotometer (Shimadzu UV-1750). The inductively coupled plasma optical emission spectrometry (ICP-OES) was tested by PerkinElmer Avio™ 200.

Electrochemical NRR measurements

The electrochemical experiments were conducted on a Bio-Logic VMP3 potentiostat system by using a three-electrode configuration (carbon paper loaded with catalyst as working electrode, carbon electrode as counter electrode, and Ag/AgCl/saturated KCl as reference electrode). The electrolytic cell is H-type cell, in which the two-compartment electrochemical cell is separated by the proton exchange membrane Nafion 117. The Nafion 117 membrane was preconditioned by boiling in 5% H_2O_2 solution and ultrapure water at 80 °C for 1 h respectively, and then sonicated

in 0.05 M H_2SO_4 and ultrapure water for 1 h, respectively. All potentials were converted to reversible hydrogen electrode (RHE). For electrochemical NRR, potentiostatic tests were carried out in 0.1 M potassium hydroxide solution as the electrolyte, which was purged with ultra-high purity N_2 (99.999%) for 30 min before the NRR measurement. Pure N_2 with a constant flow rate of 20 mL min^{-1} was continuously fed into the cathodic compartment with a properly positioned sparger during the experiments. Linear sweep voltammogram (LSV) measurements were performed from 0.5 V to −0.8 V vs. RHE at a scan rate of 5 mV s^{-1}. For NRR experiments, potentiostatic tests were conducted at different potentials ranged from −0.3 V to 0 V vs. RHE for 2 h. After the entire reduction reaction was terminated, the electrolyte was collected to detect the ammonia product.

Cathode preparation

Typically, 2 mg catalyst and 30 μL of Nafion solution (5 wt%) were dispersed in 970 μL of absolute ethanol by sonicating for 0.5 h to form a homogeneous ink. And then, the dispersion of homogeneous ink was loaded onto a carbon paper electrode with area of 1*1 cm^2 and dried under ambient condition.

Determination of ammonia

The absorbance of the tested electrolyte was detected by Nessler's reagent color development method to determine the ammonia concentration generated after electrolysis.[2] In order to accurately quantify the ammonia produced, a standard curve of ammonia was tested first. A certain amount of ammonium chloride was weighed and dissolved in 0.1 M potassium hydroxide, and ammonia standard solutions with different concentrations (0.0, 0.2, 0.4, 0.6, 0.8 μg mL^{-1}) were

prepared in a volumetric flask. 5 mL of the above standard solution was taken, followed by adding 5 mL of 0.1 M KOH. In order to prevent the possible influence of metal ions in the solution on the color development, 1 mL of 0.2 M potassium sodium tartrate solution was added first, and then 1 mL of Nessler's reagent was added. The mixed solution was shaken and left in a dark place for 30 min to develop color. The configuration of the control blank solution was the same as above, except that 5 mL of the standard solution was replaced with 5 mL of 0.1 M potassium hydroxide. Finally, the test solution and the control blank solution were put into the cuvette to test the UV absorbance. As shown in Figure S5, according to the absorbance of standard solutions with different concentrations at 420 nm, the standard curve of ammonia concentration and absorbance was obtained by fitting. The absorbance of the tested electrolyte was measured after the above-mentioned color development steps, and the corresponding ammonia concentration can be calculated by substituting it into the standard curve.

Determination of hydrazine

The hydrazine presented in the electrolyte was estimated by the method of Watt and Chrisp. A mixture of para-(dimethylamino) benzaldehyde (5.99 g), hydrochloride (concentrated, 30 mL) and ethanol (300 mL) was used as a color reagent. 3 mL of the above prepared color reagent was added into 3 mL electrolyte and then was stirred for 10 min at room temperature in darkness. The absorbance of hydrazine in the resulting electrolyte was estimated at 460 nm. Absolute calibration of this method was achieved using hydrazine monohydrate solutions of known concentration as standards, and the fitting curve showed good linear relation of absorbance with $N_2H_4 \cdot H_2O$ concentration ($y = 0.945x - 0.00236$, $R^2 = 0.9999$) by three times independent calibrations (Figure S6).

Calculation of NH_3 yield and Faradaic efficiency:

The NH_3 yield was determined using the following equation:

$$r(NH_3) = (c \times V) / (t \times A)$$

where c is the measured NH_3 concentration, V is the volume of the electrolyte, t is the reduction reaction time, and A is the effective area of the electrode, which is the geometric area of the electrode covering with catalyst.

The Faradaic efficiency was calculated as follows:

$$FE = 3F \times c \times V / (17 \times Q)$$

where F is the Faraday constant (96500 C mol^{-1}), c is the measured NH_3 concentration, V is the volume of the electrolyte or acid trap, t is the reduction reaction time, M is the relative molecular mass of NH_3 and Q is the total charge used for the electrodes. The total ammonia production is calculated as the summary of the ammonia products in cathode chamber, anode chamber, and also in-line acid traps.

Measurement of electrochemically active surface area:

The electrochemically active surface area was measured by double layer capacitance method. CV measurement was conducted at the potential window 0.91−1.01 V vs. RHE under different scan rates of 10, 20, 30, 40, 50 mV s^{-1}. By plotting the (Ja-Jc)/2 at 0.96 V vs. RHE against the scan rate, the slope value was calculated to be the double layer capacitance (Cdl).

Supplementary Figures

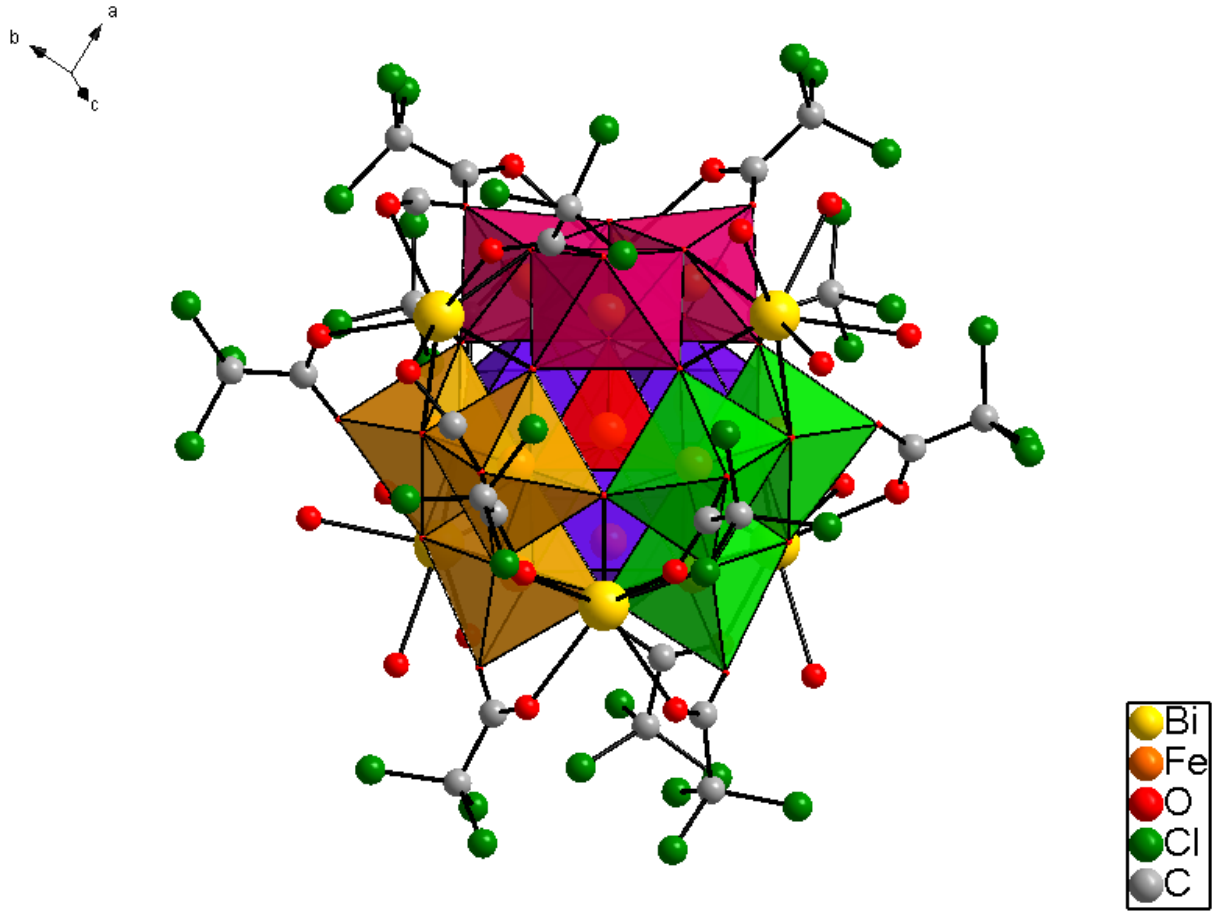

Fig. S1. Polyhedral representation of polyanion $Bi_6[FeO_4Fe_{12}O_{12}(OH)_{12}(O_2C(CCl_3)_{12}]^{17-}$ (Bi_6Fe_{13}).

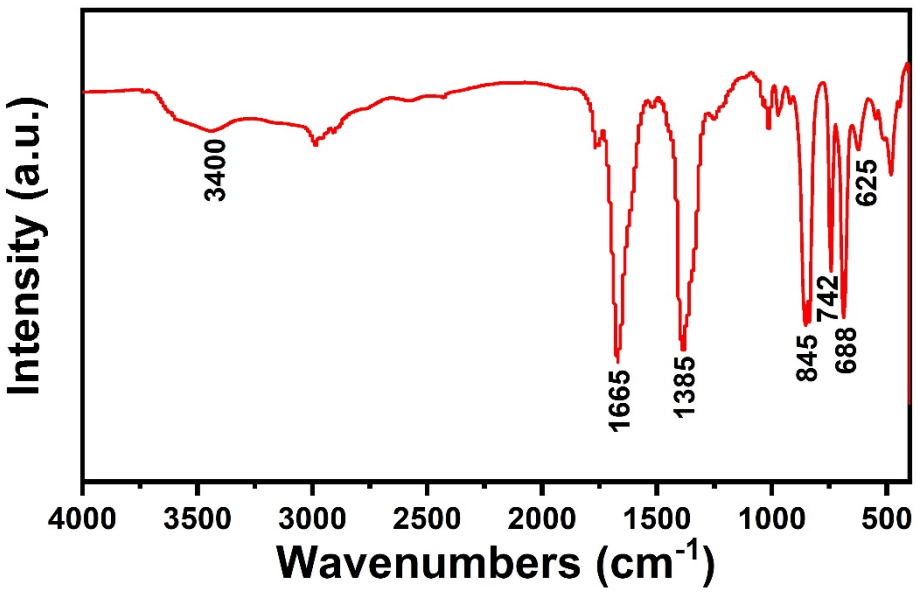

Fig. S2. IR spectrum of iron-oxo Keggin.

The broad peak at 3400 cm^{-1} is attributed to the stretching vibration absorption peak of associated O−H bond. The peak at 1665 cm^{-1} corresponds to stretching vibration of C=O bond. The peak at 1385 cm^{-1} is associated with stretching vibration of C−C bond. The peak at the 742 cm^{-1} position is a stretching vibration of C−Cl bond. The peaks at 845 cm^{-1} and 688 cm^{-1} correspond to the Bi−O bond. The absorption peak at 625 cm^{-1} corresponds to the Fe−O bond.

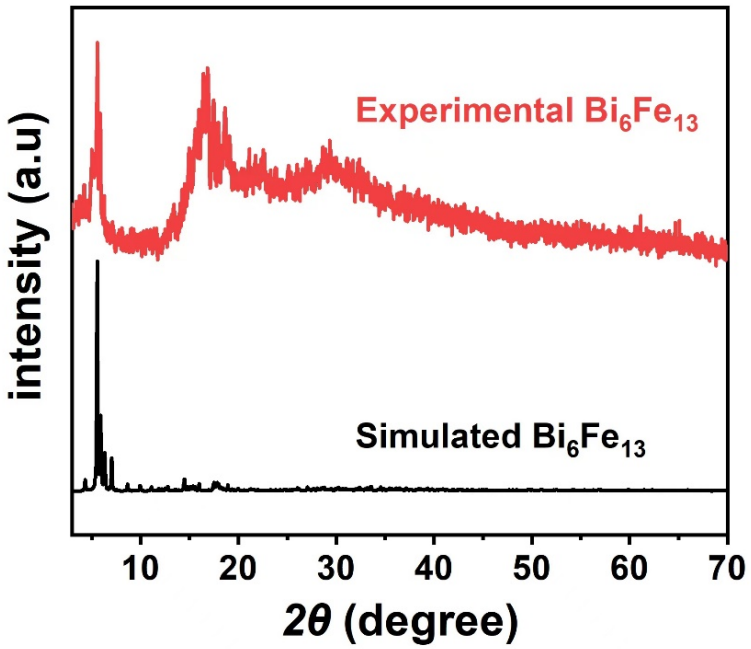

Fig. S3. XRD pattern of Bi_6Fe_{13}.

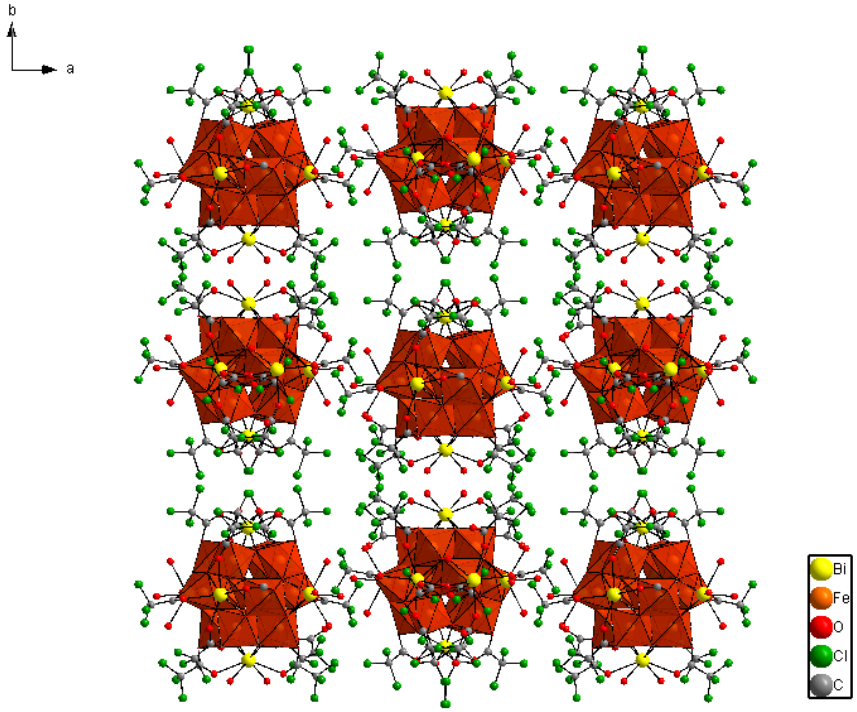

Fig. S4. Packing of Bi_6Fe_{13} along *c* direction.

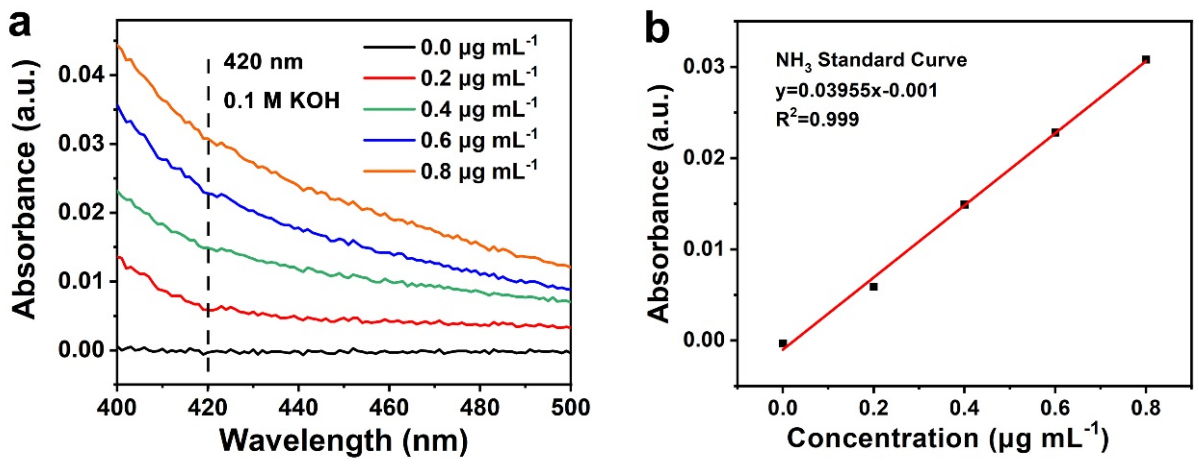

Fig. S5. UV-vis curves (a) and calibration curve (b) for the colorimetric NH_3 assay within low concentration ranges from 0.0 μg mL^{-1} to 0.8 μg mL^{-1} using the Nessler's reagent.

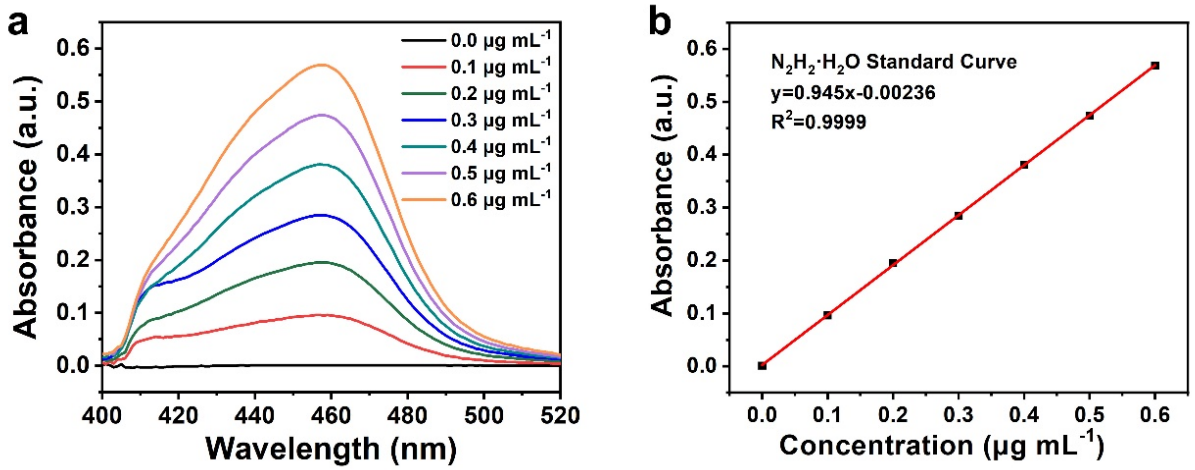

Fig. S6. (a) UV-vis curves of various $N_2H_4 \cdot H_2O$ concentrations after incubation for 10 min at room temperature and the (b) calibration curve used for the estimation of the $N_2H_4 \cdot H_2O$ concentration.

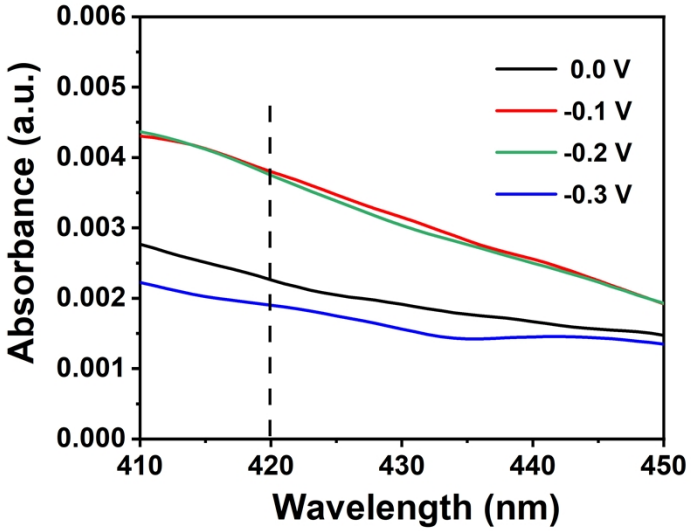

Fig. S7. UV-vis absorption spectra of Bi/BiClO/Fe_3O_4-600 electrolysis after 2 h of electrolysis at different applied potentials.

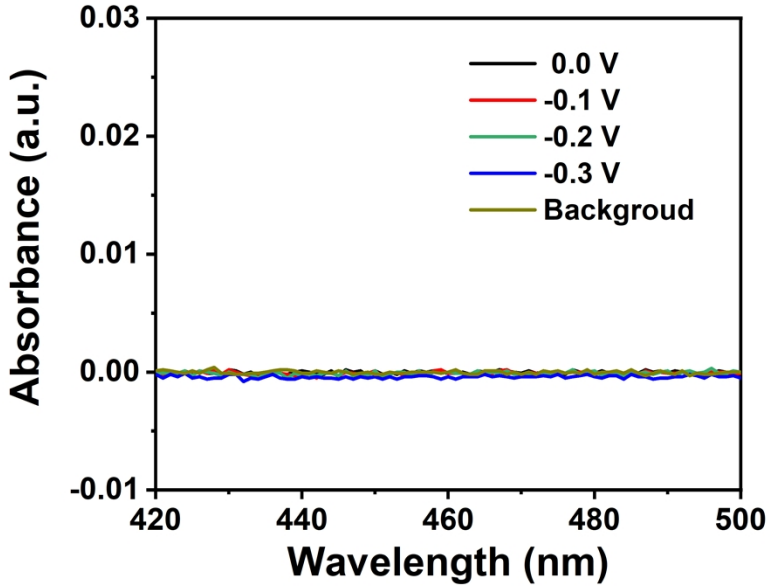

Fig. S8. (a) UV-vis absorption spectra and (b) chromogenic reaction of the electrolyte stained with the indicator for $N_2H_4 \cdot H_2O$.

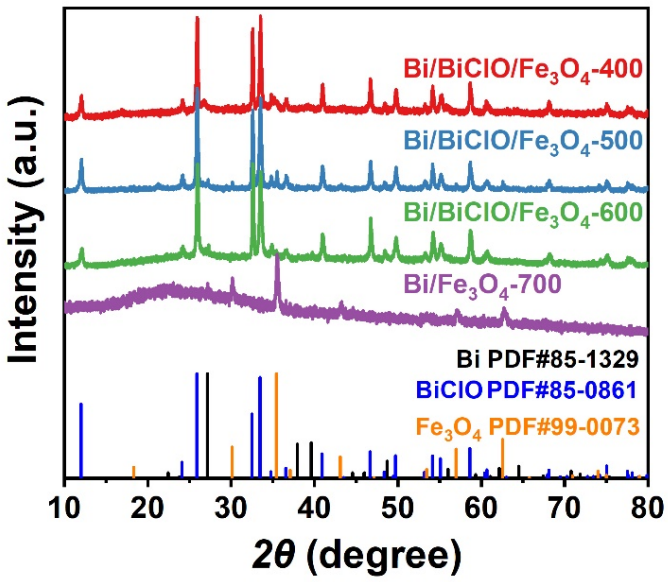

Fig. S9. X-ray diffraction patterns of samples calcined at 400 °C, 500 °C, 600 °C and 700 °C, which are donated as Bi/BiClO/Fe_3O_4-400, Bi/BiClO/Fe_3O_4-500, Bi/BiClO/Fe_3O_4-600, and Bi/Fe_3O_4-700, respectively.

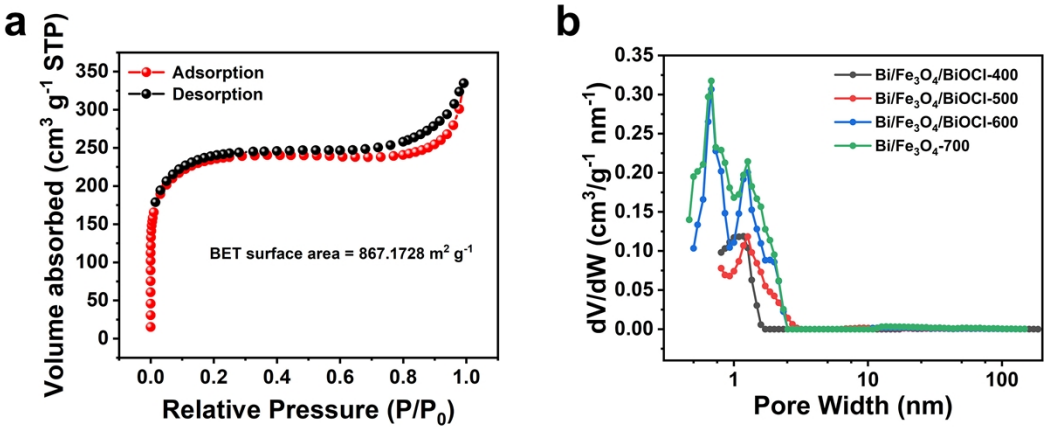

Fig. S10. (a) Nitrogen adsorption–desorption isotherms of Bi/Fe_3O_4-700. (b) Pore size distributions for Bi/BiClO/Fe_3O_4-400, Bi/BiClO/Fe_3O_4-500, Bi/BiClO/Fe_3O_4-600 and Bi/Fe_3O_4-700.

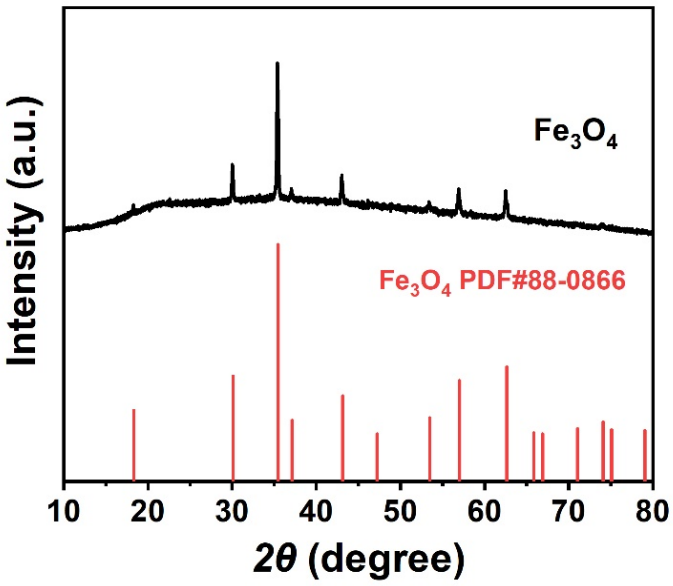

Fig. S11. X-ray diffraction pattern of Fe_3O_4.

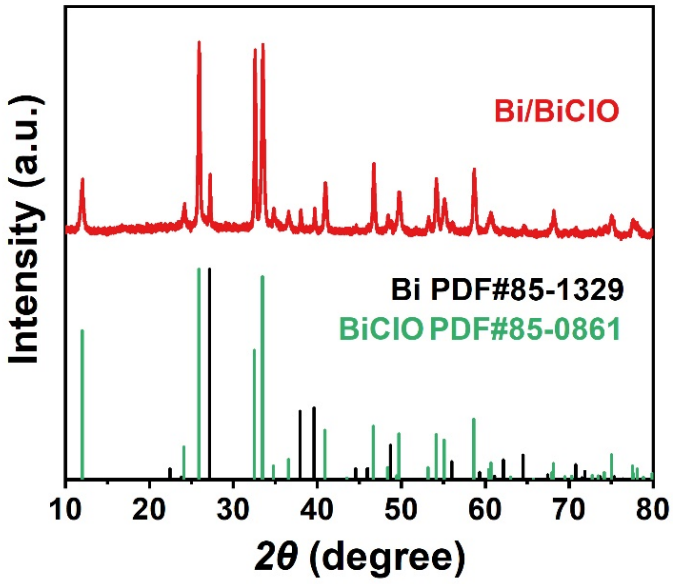

Fig. S12. X-ray diffraction pattern of Bi/BiClO.

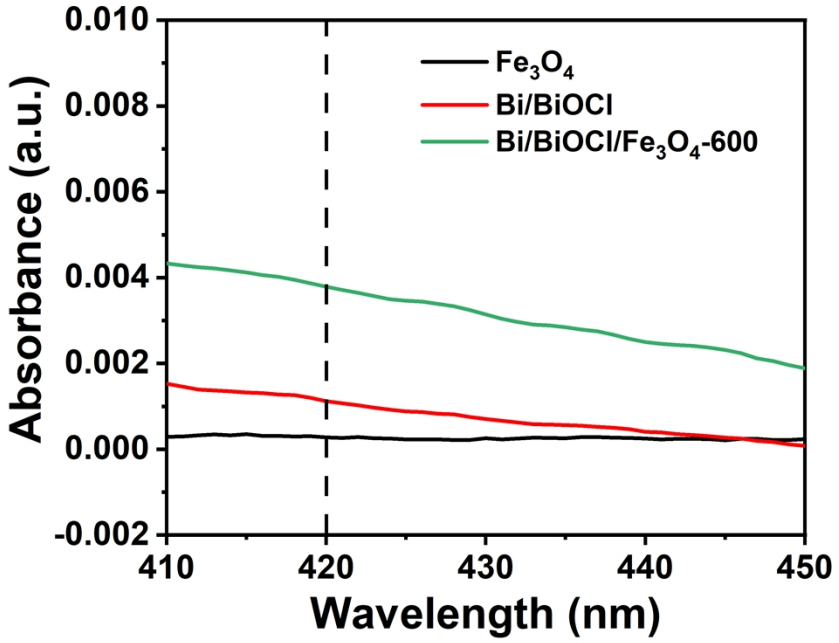

Fig. S13. UV-vis absorption spectra of Bi/BiClO/Fe_3O_4-600, Bi/BiClO, and Fe_3O_4 samples.

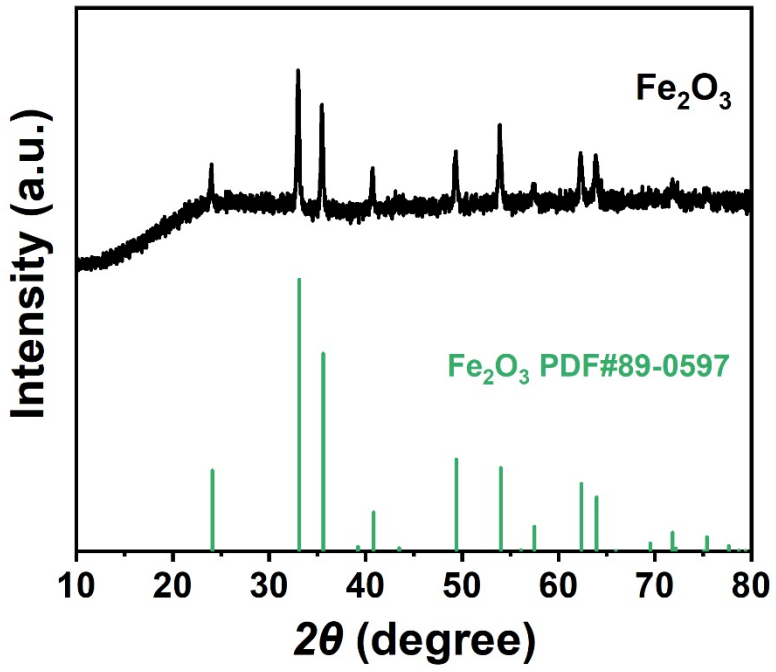

Fig. S14. X-ray diffraction pattern of Fe_2O_3.

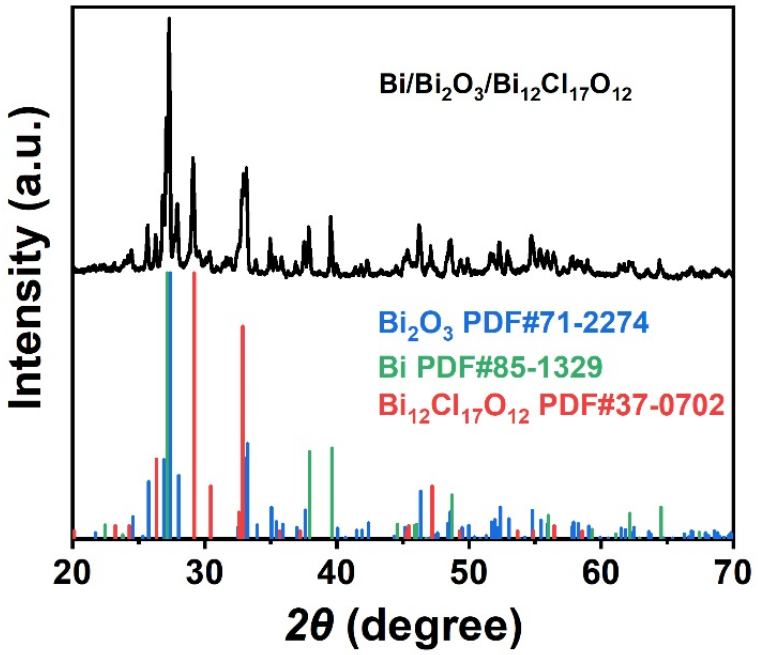

Fig. S15. X-ray diffraction pattern of $Bi/Bi_2O_3/Bi_{12}Cl_{17}O_{12}$.

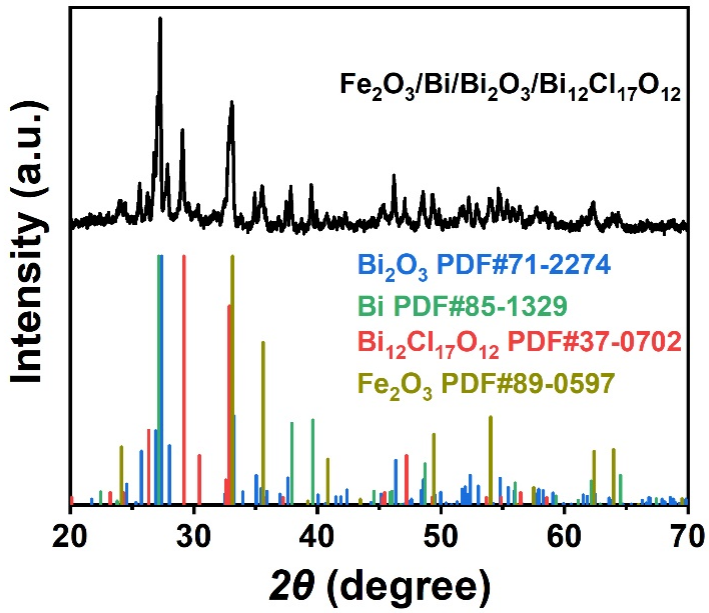

Fig. S16. X-ray diffraction pattern of $Fe_2O_3/Bi/Bi_2O_3/Bi_{12}Cl_{17}O_{12}$。

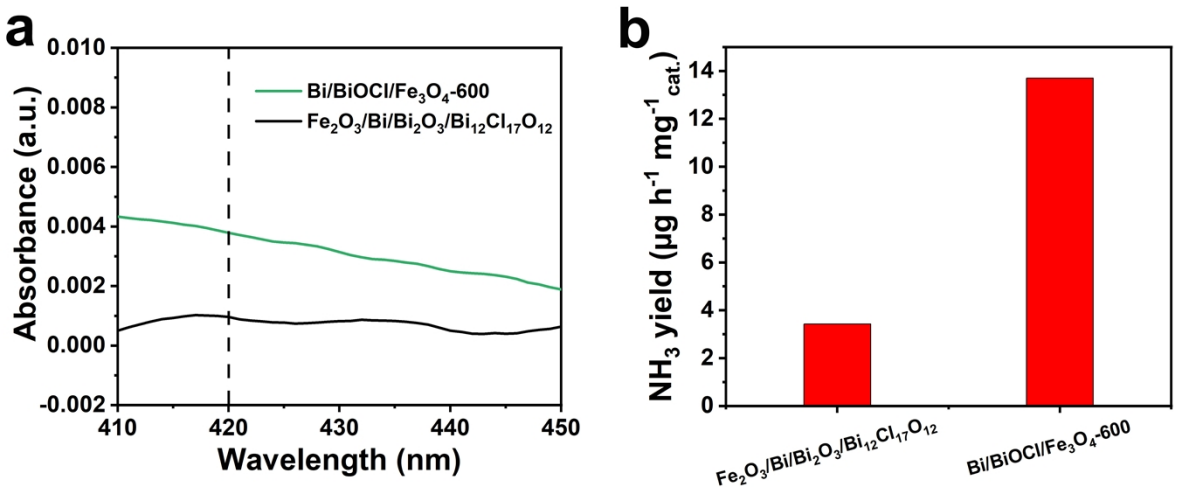

Fig. S17. (a) UV-vis absorption spectra and (b) NH_3 yields of $Fe_2O_3/Bi/Bi_2O_3/Bi_{12}Cl_{17}O_{12}$ and $Bi/BiOCl/Fe_3O_4$.

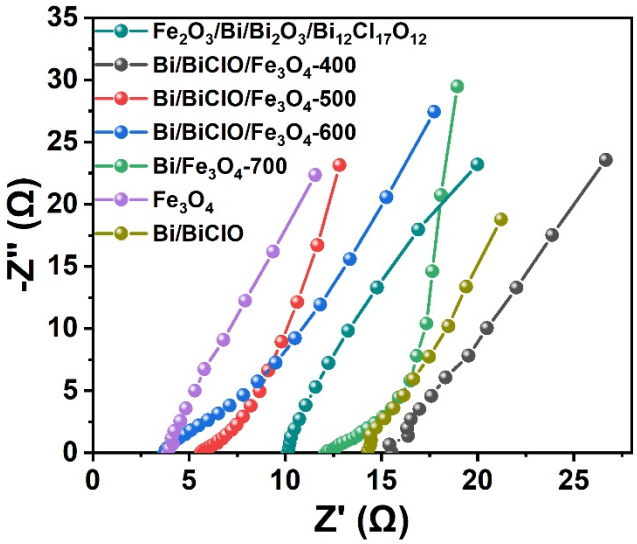

Fig. S18. Electrochemical impendence spectra of Bi/BiClO/Fe_3O_4-400, Bi/BiClO/Fe_3O_4-500, Bi/BiClO/Fe_3O_4-600, Bi/Fe_3O_4-700, Fe_3O_4, Bi/BiClO, and Fe_2O_3/Bi/Bi_2O_3/$Bi_{12}Cl_{17}O_{12}$.

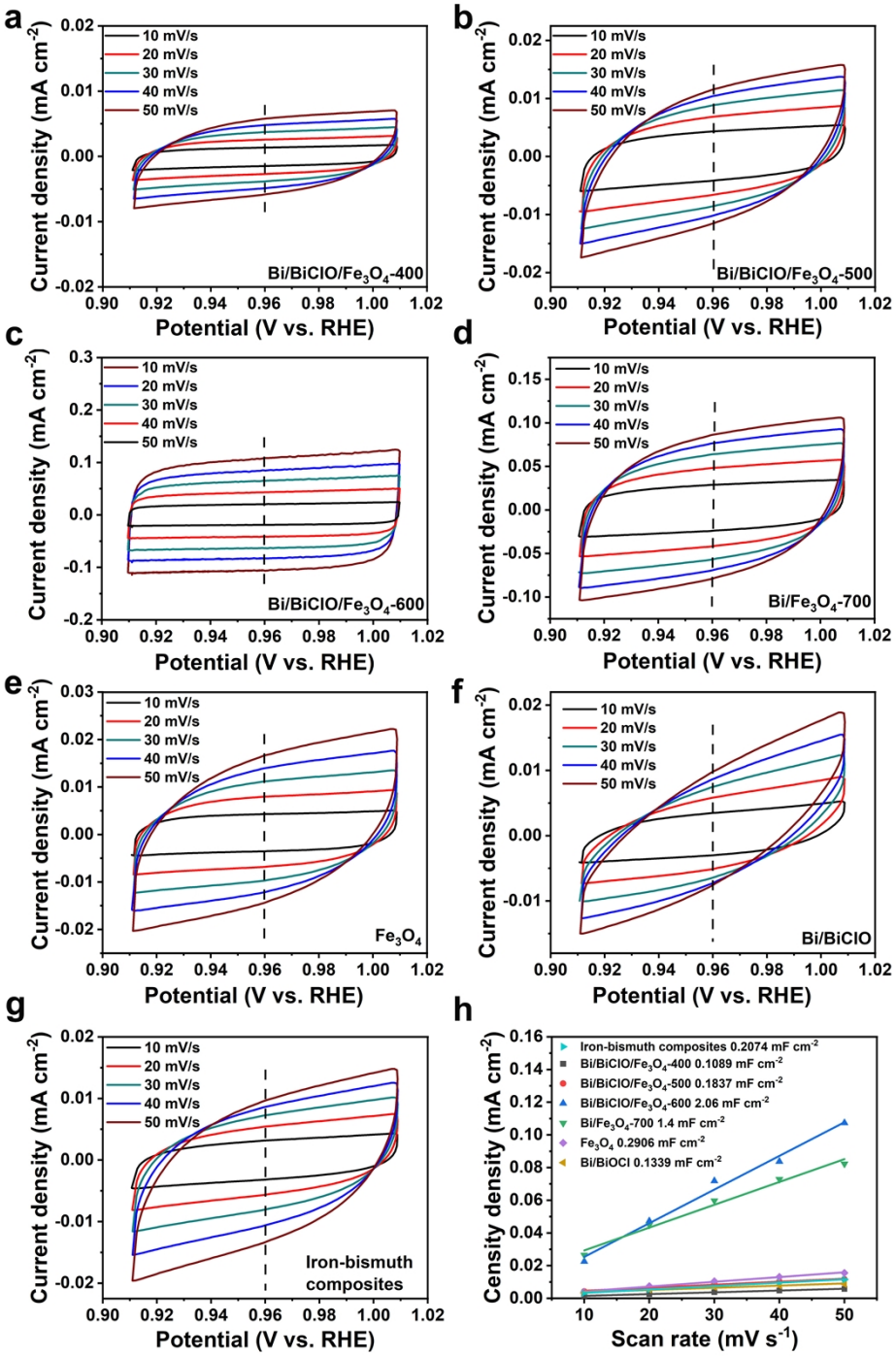

Fig. S19. Cyclic voltammograms with different scanning rates of 10, 20, 30, 40 and 50 mV s^{-1} for (a) Bi/BiClO/Fe_3O_4-400, (b) Bi/BiClO/Fe_3O_4-500, (c) Bi/BiClO/Fe_3O_4-600, (d) Bi/Fe_3O_4-700, (e) Fe_3O_4, (f) Bi/BiClO, and (g) Fe_2O_3/Bi/Bi_2O_3/$Bi_{12}Cl_{17}O_{12}$. (h) Corresponding plots of current density at −0.96 V versus the scan rate.

Table S1. The mass and molar ratios of Bi/BiClO/Fe_3O_4-400, Bi/BiClO/Fe_3O_4-500, Bi/BiClO/Fe_3O_4-600, and Bi/Fe_3O_4-700 measured from ICP-OES results.

Catalysts	Fe (wt%)	Bi (wt%)	Fe/Bi atomic ratio
Bi/BiClO/Fe_3O_4-400	16.04	63.88	0.937
Bi/BiClO/Fe_3O_4-500	34.6	43.86	2.944
Bi/BiClO/Fe_3O_4-600	41.75	41	3.800
Bi/Fe_3O_4-700	75	10	27.991

Table S2. Comparison of the Bi/BiClO/Fe_3O_4-600 with various other electrocatalysts for the electrochemical production of NH_3 from N_2 under ambient conditions.

Electrocatalyst	Electrolyte	Potential (V vs. RHE)	NH_3 yield rate ($\mu g\ h^{-1}\ mg^{-1}_{cat.}$)	NH_3 Faradaic efficiency	Reference
Bi/BiClO/Fe_3O_4-600	**0.1 M KOH**	**-0.1**	**12.82**	**15.22%**	**This work**
Fe/Cu	0.1 M KOH	-0.1	22.6	16%	Mater. Today Energy, 2023, 31, 101215.
Fe/Mo NC	0.1 M Na_2SO_4	-0.6	26.8	11.8	Nano Res, 2022, DOI: 10.1007/s12274-022-5246-x.
D-FeN/C	0.1 M KOH	-0.4	24.8	15.8	Adv. Funct. Mater., 2022, 32, 2205409
FeTPPCl	0.1 M Na_2SO_4-PBS	-0.3	18.28	16.76	Appl. Catal., B, 2021, 285, 119794.
Bi nanosheet	0.1 M Na_2SO_4	-0.8	13.23	10.46%	ACS Catal., 2019, 9, 2902
Fe–N/CNT	0.1 M KOH	-0.2	34.83	9.2%	ACS Catal., 2019, 9, 336
α-Fe_2O_3/CNT	0.1 M KOH	-0.11	0.43	8.3%	Chem. Eur. J., 2018, 24, 1
Fe_3O_4/Ti	0.1 M Na_2SO_4	-0.4	4.63	2.6%	Nanoscale, 2018, 10, 14386

References:

1. P. Singhal, S. K. Jha, S. P. Pandey and S. Neogy, Rapid extraction of uranium from sea water using Fe_3O_4 and humic acid coated Fe_3O_4 nanoparticles, *J. Hazard. Mater.*, 2017, **335**, 152–161.
2. Y. Wang, X. Cui, J. Zhao, G. Jia, L. Gu, Q. Zhang, L. Meng, Z. Shi, L. Zheng, C. Wang, Z. Zhang and W. Zheng, Rational Design of Fe-N/C Hybrid for Enhanced Nitrogen Reduction Electrocatalysis under Ambient Conditions in Aqueous Solution, *ACS Catal.*, 2019, **9**, 336–344.